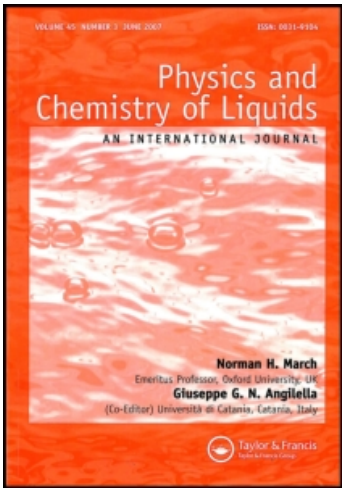

Physics and Chemistry of Liquids
Publication details, including instructions for authors and subscription information:
http://www.informaworld.com/smpp/title~content=t713646857

Microscopic Motion of Atoms in Simple Liquids at Equilibrium and with Shear Flow

D. M. Heyes[a]; W. C. Sandberg[ab]
[a] Department of Chemistry, Royal Holloway and Bedford New College, University of London, Egham, Surrey, UK [b] Laboratory for Computational Physics and Fluid Dynamics, Naval Research Laboratory, Washington, DC, USA

To cite this Article Heyes, D. M. and Sandberg, W. C.(1990) 'Microscopic Motion of Atoms in Simple Liquids at Equilibrium and with Shear Flow', Physics and Chemistry of Liquids, 22: 1, 31 — 50
To link to this Article: DOI: 10.1080/00319109008036409
URL: http://dx.doi.org/10.1080/00319109008036409

Phys. Chem. Liq., 1990, Vol. 22, pp. 31–50
Reprints available directly from the publisher
Photocopying permitted by license only

MICROSCOPIC MOTION OF ATOMS IN SIMPLE LIQUIDS AT EQUILIBRIUM AND WITH SHEAR FLOW

D. M. HEYES and W. C. SANDBERG†

Department of Chemistry, Royal Holloway and Bedford New College, University of London, Egham, Surrey TW20 OEX, UK.

(Received 31 January 1990)

We investigate the microscopic mechanism of atomic motion and local stress relaxation in Lennard-Jones, *LJ* liquids using a *new* class of correlation functions that emphasise the interplay between an abitrary atom in the fluid and its surrounding shells of atoms. We use the linear momenta and stress tensor to characterise the time dependence of this interaction. We consider a series of correlation functions that give complementary information and build a picture of the single particle and small cluster motion. The central particle and first shell undergo a reversal in momentum at **different** times after the 'collision' of the central particle and its first shell of neighbours. This 'phase difference' becomes manifest in the subsequent dynamics probed by the new correlation functions. We also consider the effect of a non-newtonian shear flow on this local dynamical relaxation, using profile biased laminar flow equations of motion. In non-newtonian shear flow we find the momentum transfer between particle and cage to be less pronounced and occur over a wider time range.

KEY WORDS: Lennard-Jones interactions, stress tensor, non-Newtonian flow.

1 INTRODUCTION

Understanding the motion of small groups of atoms in simple fluids has been an ongoing application of molecular dynamics computer simulation, *MD*, since the pioneering work of Rahman,[1] (followed up by Franchetti[2]) and Alder and Wainwright[3]. In the more recent past some highlights are, for example, a (progessively refined) viscoelastic theory of the momentum autocorrelation and momentum trans-transfer functions, written in terms of the longitudinal and transverse momentum current density correlation functions, developed by Gaskell and co-workers[4,5]. At a more empirical level, single particle trajectories and their relationship with the surrounding cage have been analysed directly by *MD*. A decomposition of the momentum autocorrelation function from particles initially in high and low local density conditions showed a more oscillatory appearance in the initially low density environment[6]. Recollision probabilities have also been investigated; recollision with the same particle is highly probable[7]. Haan and others showed that the time evolution of the separation of pairs of atoms in a simple fluid satisfied the Smoluchowski's

† Permanent address: Laboratory for Computational Physics and Fluid Dynamics, Naval Research Laboratory, Washington, DC 20375-5000, USA.

equation with a potential of mean force[8,9]. Two, three and higher particle regroupings of relevance to stress relaxation in simple fluids have also been considered, both implicitly in terms of the local free volume[10] and directly[11]. In the latter study, the long-time decay of the shear-stress autocorrelation function is shown to be determined primarily by a **reorientation** of the 'bonds' connecting the close neighbours. Kushick and co-workers showed that the principle role of the attractive forces is to enhance the cohesiveness and longevity of the cage, giving rise to a much deeper momentum autocorrelation function from enhanced coherence between 'backscattering' events[12]. A longitudinal resolution of the momentum transfer cross-correlation function showed that at short times transfer of the momentum is primarily in the longitudinal direction. As the momentum spreads within the first shell and beyond, the contribution from the transverse modes increases[13]. There have been a number of treatments of the momentum autocorrelation function using the generalised Langevin equation solved with a variety of prescriptions for the time-dependent friction coefficient[14]. It is clear from treatments of extensive analyses of single particle motion in simple fluids[15] and self-diffusion in simple molecular fluids[16] that the attractive part of the potential has a strong influence on the molecular diffusion mechanism largely through the change in the dynamics of the particle cages.

These studies, considered overall, reveal that the interaction between the atom and its **non-stationary** cage—the key to any understanding of local dynamical relaxation—is still poorly characterised. None of these studies **directly** addresses this correlation. Despite many papers on this subject, there are still important unanswered questions. We make further progress with the assistance of a number of *new* specifically designed time correlation functions which probe hitherto unstudied aspects of the interplay between the fluid atoms and their cages in simple fluids. It is important to look at several correlation functions from the same state point, as a single correlation function can often be misleading in promoting a particular view of the single particle dynamics. This is because any particular correlation function uses **one** physical property to probe the dynamics. By the analytic formula for this property it will weight certain dynamical events more than others. The force autocorrelation function, for example, emphasises those points in time when the particle is subjected to a large repulsive force.

2 THEORY AND SIMULATION METHOD

We define three classes of particle for the purposes of resolving the momenta and stress around a central particle. (All N particles in the simulation cell are considered as being 'central' particles in turn, at each time origin. A time origin is commenced each time step.) The central particle or 'impurity' we give the generic subscript, 1. Particles lying within an annulus of inner and outer radii, r_a and r_b, respectively about the central particle at arbitrary time are given the subscript, 2. Particles lying within an annulus of inner and outer radii, r_b and r_c, respectively about the central particle are similarly given the subscript, 3. The nearest shell S_1 comprised of '2' atoms, has a total momentum which is simply the sum of the component momenta of the particles

lying within that radial separation at the time of interest, i.e.,

$$p_2 = \sum_{j \neq 1, r_a < r_{1j} < r_b}^{N_{S1}} p_j, \tag{1}$$

where r_{1j} is the separation between the central particle, 1 and a neighbour of index, j, and N_{S1} is the total number of atoms in shell 1. N_{s1} will vary somewhat with time. (The mass of the particle is unity in the units considered here. Therefore the momentum and velocity of a single particle are numerically the same.) The cross-correlation functions between the momenta of the central particle and the nearest shell of neighbours is,

$$C_{12}(t) = \langle p_1(0) p_2(t) \rangle. \tag{2}$$

As time progresses the neighbours about particle 1 lying within r_a and r_b can change. An alternative prescription would be to maintain the same neighbours for each particle during the correlation process. This would cause the shape of the shell to distort with time from spherical symmetry at the time of origin. We do not adopt this latter approach, because as momentum relaxation and diffusion occur on disparate time scales ('fast' and 'slow', respectively) and shell will remain virtually intact throughout the duration of the correlation. Any attempt to maintain the same particles as 'shell' particles for each central particle during the length of the correlation would be an unnecessary and technically time-consuming complication. The momentum of shell 2 (i.e., S_2), which compromised of '3' atoms, is the sum of the component velocities within that radial separation at the time of interest, i.e.,

$$p_3 = \sum_{j \neq 1, r_b < r_{1j} < r_c}^{N_{S2}} p_j. \tag{3}$$

where again N_{s2} is variable. The cross-correlation function between the central particle and the next defined shell of neighbours is,

$$C_{13}(t) = \langle p_1(0) p_3(t) \rangle. \tag{4}$$

The advantage of following the behaviour of two shells, rather than one (as has been customary to date) is that it gives a better insight into the transfer of momentum and stress around and from the central particle.

We also investigate the relative momentum correlation functions,

$$C^{12}(t) = \langle (p_1(0) - p_2(0))(p_1(t) - p_2(t)) \rangle, \tag{5}$$

$$C^{13}(t) = \langle (p_1(0) - p_3(0))(p_1(t) - p_3(t)) \rangle, \tag{6}$$

and,

$$C^{23}(t) = \langle (p_2(0) - p_3(0))(p_2(t) - p_3(t)) \rangle. \tag{7}$$

The definition of our shell-time correlation functions is the same as that of Balucani *et al.*[13] in that we omit the central particle in our definition of the 'shell' momenta. This gives a clear separation of the relative dynamics between the central particle and its first shell. In particular we are able to identify the phase difference

in the motion of the central particle with respect to the first shell. In some of their papers Gaskell and co-workers have adopted an alternative definition of the first shell, which includes the central particle in the definition of the shell.[17,18]

The MD simulations followed particles of mass, m, interacting via the Lennard-Jones, *LJ*, potential[19],

$$\phi(r) = 4\varepsilon((\sigma/r)^{12} - (\sigma/r)^{6}), \tag{8}$$

The basic technique is that used in a previous *MD* study[19–21]. The MD simulations were performed on a cubic unit cell of volume V containing either $N = 256$ or $N = 500$. The interactions were truncated at 2.5σ. We use LJ reduced units throughout, i.e., $k_B T/\varepsilon \to T$, and number density, $\rho = N\sigma^3/V$. Time is in $\sigma(m/\varepsilon)^{1/2}$, shear strain rate is in $(\varepsilon/m)^{1/2}/\sigma$, viscosity is in $(m\varepsilon)^{1/2}/\sigma^2$ and pressure tensor components or stress are in $\varepsilon\sigma^{-3}$. Simulations were conducted for typically 25,000 time steps of duration 0.015 reduced time units.

Some of the simulations had a superimposed shear flow on the dynamics. We used the SLLOD algorithm to impose a shear flow on the molecules[20,21]. The peculiar or thermal momentum is denoted by $\tilde{p}$. For molecular position, $\underline{R}$,

$$\dot{R}_X = p_X/m = \tilde{p}_X/m + \dot{\gamma}R_Y/m, \tag{9}$$

$$\dot{R}_Y = p_Y/m = \tilde{p}_Y/m, \tag{10}$$

$$\dot{R}_Z = p_Z/m = \tilde{p}_Z/m, \tag{11}$$

$$\frac{d\tilde{p}_x}{dt} = F_X - \dot{\gamma}\tilde{p}_Y, \tag{12}$$

$$\frac{d\tilde{p}_Y}{dt} = F_Y, \tag{13}$$

$$\frac{d\tilde{p}_Z}{dt} = F_Z, \tag{14}$$

where the α component of the force on a particle is F_α, the momentum is p_α, the peculiar momentum is $\tilde{p}_\alpha$ (i.e., that component of the momentum in excess of the streaming flow momentum). We maintain constant kinetic energy ('temperature') within the Verlet algorithm using *momentum* rescaling applied to $\tilde{p}_\alpha$. In order to assess the stress relaxation around the central molecule, we define a single particle stress for our generic particle 1 (i.e., each of the N particles in turn),

$$\sigma_{1\alpha\beta} = \frac{N}{V}\left(m_1\bar{v}_{\alpha 1}\bar{v}_{\beta 1} - (1/2)\sum_{j\neq 1}(r_{\alpha 1 j}r_{\beta 1 j}/r_{1j})\frac{d\phi(r_{1j})}{dr}\right), \tag{15}$$

where $r_{\alpha 1 j}$ is the α component of $\underline{r}_{1j}$ and $V = (N/\rho)$, the volume of the MD cell. The stress of the first 'shell', (i.e., S_1) is the sum of the 'component' stresses within that radial separation at the time of interest, i.e.,

$$\sigma_2 = \sum_{j\neq 1, r_a < r_{1j} < r_b}^{N_{S1}} \sigma_j. \tag{16}$$

The cross-correlation function between the 'stress' on the central particle and that on the first defined shell of neighbours is,

$$S_{12}(t) = \langle \sigma_1(0)\sigma_2(t)\rangle. \tag{17}$$

and for the central particle on the next shell, S_2,

$$S_{13}(t) = \langle \sigma_1(0)\sigma_3(t)\rangle, \tag{18}$$

using,

$$\sigma_3 = \sum_{j\neq 1, r_b < r_{1j} < r_c}^{N_{S1}} \sigma_j. \tag{19}$$

We also make use of $S_{11}(t)$ and $S_{22}(t)$ in our discussion,

$$S_{11}(t) = \langle \sigma_1(0)\sigma_1(t)\rangle, \tag{20}$$

and,

$$S_{22}(t) = \langle \sigma_2(0)\sigma_2(t)\rangle. \tag{21}$$

We calculated the shear viscosity, η, from,

$$\eta = -P_{XY}/\dot{\gamma}, \tag{22}$$

where,

$$P_{XY} = \frac{1}{V}\left(\sum_{i=1}^{N} m_i \tilde{v}_{xi}\tilde{v}_{yi} - \sum_{i=1}^{N-1}\sum_{j>i}^{N} (r_{xij}r_{yij}/r_{ij})\frac{d\phi(r_{ij})}{dr}\right), \tag{23}$$

where r_{xij} is the x component of $\underline{r}_{ij}$ and $V = (N/\rho)$, the volume of the MD cell. The state point mainly considered was a near triple point state, at $\rho = 0.8442$ and $T = 0.722$. In the sheared case, $\dot{\gamma} = 1.0$, produces $\eta = 2.1$. This is about 30% shear viscosity reduction or shear thinning from the newtonian value (i.e. $\dot{\gamma} \to 0$)[19]. The stress and thermodynamic properties are governed mainly by the configurational (i.e., $\phi(r)$) dependent terms at this state point.

Computations were carried out in single precision on a CRAY-XMP at the University of London Computer Centre.

3 RESULTS AND DISCUSSION

At equilibrium and steady state shear we evaluated the single particle autocorrelation functions, $\langle \tilde{p}_X(0)\tilde{p}_X(t)\rangle$, $\langle \tilde{p}_Y(0)\tilde{p}_Y(t)\rangle$, $\langle \tilde{p}_Z(0)\tilde{p}_Z(t)\rangle$, $\langle F_X(0)F_X(t)\rangle$, $\langle F_Y(0)F_Y(t)\rangle$, $\langle F_Z(0)F_Z(t)\rangle$. We also computed, $C^{12}(t)$, $C^{13}(t)$, $C^{23}(t)$, $C_{12}(t)$, $C_{13}(t)$, $C_{23}(t)$, resolved into X, Y and Z components. The $S_{12}(t)$, $S_{13}(t)$, $S_{23}(t)$ are resolved into, XX, YY, ZZ, XY, XZ, YZ components.

In Figure 1 we compare the normalised momentum and force autocorrelation functions, $C_p(t)$ and $C_F(t)$ with the relative momentum correlation function, $C^{12}(t)$ for $\rho = 0.8442$ and $T = 0.722$, $\dot{\gamma} = 0$, $r_a = 0.85$, $r_b = 1.3$ and $r_c = 1.6$. The momentum

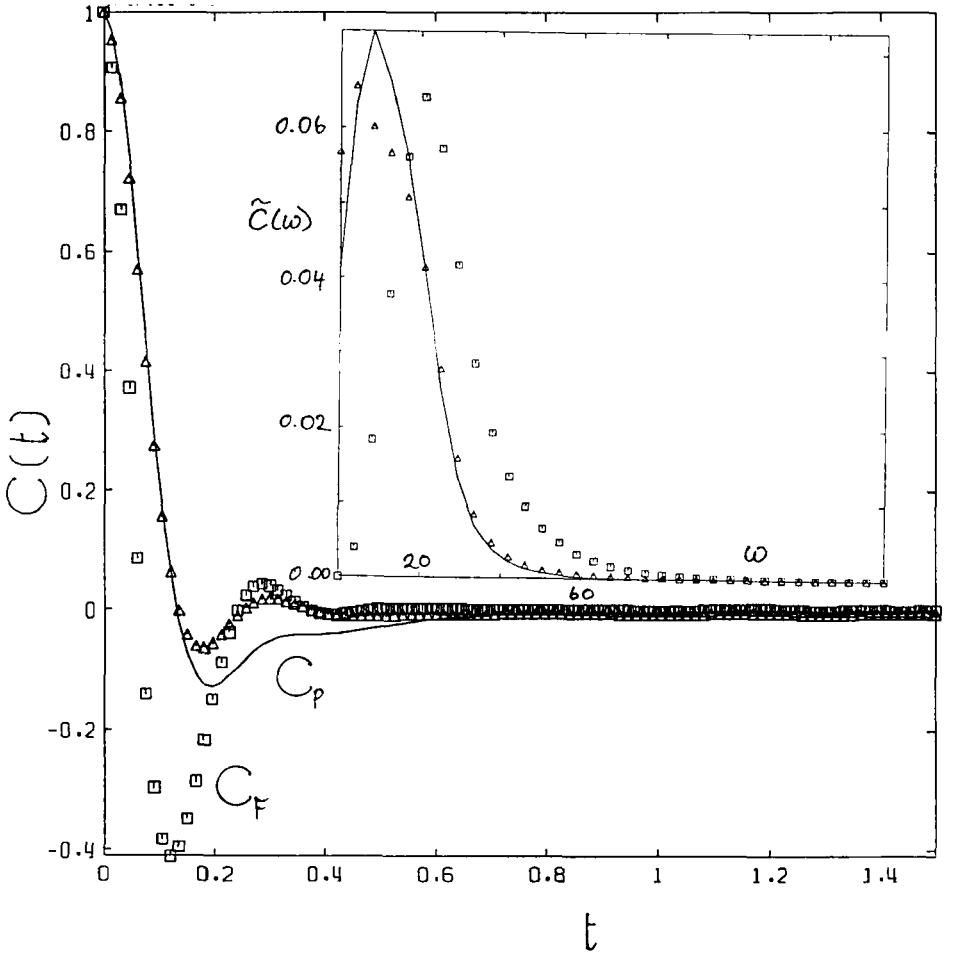

Figure 1 The x component time cross-correlation functions $C_p(t)$, solid line, $C_F(t)$, □ and $C^{12}(t)$, △, at the 3D *LJ* $N = 256$ state $\rho = 0.8442$, $T = 0.722$, $\dot{\gamma} = 0$, $r_a = 0.85$, $r_b = 1.3$ and $r_c = 1.6$. The insert shows the corresponding real frequency transforms. The second frequency moments are, 16.1, 27.6 and 19.4 ± 0.1 respectively.

and force autocorrelation functions first cross zero at $t = 0.13$ and $t = 0.07$, respectively. We point out several features which are evident in this figure. First, there is a large difference in the times at which the force and momentum autocorrelation functions first cross through zero, t_{0f} and t_{0p}, respectively. The minimum in the force autocorrelation function, facf, t_{mf}, coincides approximately with the 'cross-over' through zero time of the momentum autocorrelation function, macf. The time period, $t_{of} \rightarrow t_{pf}$, is that during which the particle is suffering a major deceleration caused by its close approach to the boundary of the first shell. The cross-over in the macf corresponds to an **on average** reversal of the particle's momentum from its value at $t \simeq 0$. Following this reversal, the facf can be seen to diminish as the repulsive force on the particle decreases. (Incidently, this fact suggests that there is an out of phase

relative motion of the central particle and first cage, S_1. That is, the central particle reverses its momentum whereas the cage continues on in the original direction of the particle. This has been suggested by Sandberg *et al.*[29] in their analysis of collision induced absorption in liquid mixtures.) The minimum in the macf corresponds to the time at which the central particle has its maximum momentum in the 'reverse' direction. We note that the facf is still negative at this time. One would expect that the minimum of the macf would coincide with the zero cross-over of the facf if the cage were stationary. However, despite a reduction in the negative momentum, the force still would appear to act in the reverse direction (implying further acceleration of the impurity in the reverse direction.). This somewhat paradoxical feature illustrates the danger of attempting to picture single particle motion by comparing different time correlation functions, here the momentum and force, which weight physical events differently. This is illustrated well by considering the $t = 0$ values of the macf and facf. They highlight those **different** times in which the momentum and force, respectively, are at a maximum—which are almost certainly not the same points in passage time of the simulation. (In a simple harmonic oscillator these are at different times.) In fact, the only value of t when one can reasonably expect there to be a coincidence of 'events' is at t_{0v}. The negative minimum of the facf heavily weights those events when their is a strong returning force on the central particle. Therefore, it is not inconsistent for the facf to remain negative while the macf starts to approach zero after the first minimum. (For a simple harmonic oscillator, the velocity and force autocorrelation functions have coincident cross-overs.) Murthy and Singer have already demonstrated the failure of a simple harmonic oscillator model for single particle motion in a simple liquid[15,22]. They showed, for example, that zeros in the acceleration are 1.5–2 times more frequent than zeros of the momentum. (In a harmonic oscillator these are equal in number.) The reason for this is because the central particle is not moving in a constant force field, but one changing through the significantly independent motion of the shell molecules.

The facf eventually returns to a positive value and subsequently decreases to zero. We suggest that this peak in the facf is associated with the approach of the central particle to the opposite side of its cage. The increasing repulsive force is reflected in the slowing decay of the macf at $t \simeq 0.3$. However, on average, the central particle does not appear to suffer a second reversal as can be seen by the absence of a second cross-over through zero of the macf. It could be that there is no momentum reversal during this interaction of the central particle with the first 'shell' because the particles on the opposite side of the cage are poorly correlated with those of the initial impact. (There is a dramatic decrease in the coherence of collisions after the first impact.)

We now discuss the relative momentum correlation function between the impurity and the first shell, which is also shown in Figure 1. At short times, (≤ 0.1), there is no discernable difference between $C^{12}(t)$ and $C_p(t)$. At short times the impurity appears to have no overall effect on the motion of S_1 and is statistically decoupled from it. There are on the average 8 neighbours in S_1 (and 4 in S_2) for the near-triple point state, $\rho = 0.8442$ and $T = 0.722$. Although the momentum transfer process begins close to $t = 0$, as shown by Balucani *et al*,[23–27] and continues for some time, the magnitude of the transferred momentum is initially insignificant due to the mass of

the shell. Each of the 8 particles will initially have velocities uncorrelated with that of the central particle. At the cross-over or 'point of impact', $t = t_{0p}$, $C^{12}(t)$ and $C_p(t)$ begin to differ. The $C^{12}(t)$ has a shallower minimum and, in contrast to $C_p(t)$, goes positive again at the point when the particle is interacting strongly with the opposite side of S_1, following closely $C_F(t)$ in this behaviour. This suggests that the shell is now moving in the same direction as the impurity, and opposite to the impurity's velocity at time $t = 0$. Therefore we suggest that the cage reverses its direction at a time $t \simeq 0.3$. This reversed motion of the shell acts, in addition, to decrease the relative separation of impurity and cage, causing the slow return of the macf, $C_p(t)$ towards zero. The shell, S_1, momentum is greater than that of the central particle when the central particle starts to interact strongly with the opposite side of S_1. The cage has a momentum in excess of the central particle as the central particle moves through the centre of the cage towards the opposite side of S_1. A positive region in $C^{12}(t)$ is the consequence of this and is consistent with the slow return to zero noted for $C_p(t)$. The insert of Figure 1 shows the power spectra of these correlation functions, $\tilde{C}_p(\omega)$ obtained using Filon's method[28]. The second frequency moment for this figure (given in the caption) are,

$$\langle \omega^2 \rangle = \frac{\int_{-\infty}^{\infty} \omega^2 \tilde{C}(\omega) d\omega}{\int_{-\infty}^{\infty} \tilde{C}(\omega) d\omega}. \tag{24}$$

The main feature of interest in this figure is the near coincidence of the $\tilde{C}^{12}(\omega)$ and $\tilde{C}_p(\omega)$ at high frequency, $\omega > 25$. As the corresponding time correlation functions are coincident until $t = 0.1$, this is consistent with the correspondence that 'short-time' is equivalent to 'high-frequency'. We note that the dominance of the short time region of the correlation function extends to high frequencies, back almost to the spectral peak. The zero crossover time have been used in estimating the location of the spectral peak associated with the dipole moment autocorrelation function.[29]

In Figure 2(a) we show the x, y and z components of the momentum transfer cross-correlation function, (MTCCF), $C_{12}(t)$, the product of central particle and first shell particle momenta. Our definition of $C_{12}(t)$ is the same of Balucani *et al.*[13] in that we omit the contribution of the central particle to the shell's momentum i.e., the macf component, $\langle p_1(0)p_1(t)\rangle$, to $C_{12}(t)$. However, unlike Balucani *et al.*[13], we have not corrected for the effects of the fixed momentum of the MD cell. (This results in a small non-zero value for $C_{12}(0)$, evident in this figure. The maximum effect of this is at $t = 0$.) The momentum transfer to the first shell rises sharply and peaks at $t = 0.12$, just prior to the zero cross-over in the macf. The subsequent decrease in $C_{12}(t)$ reflects the transfer of momentum from the first shell, S_1 to the second shell, S_2 and beyond. The zero cross-over occurs at $t = 0.28$, when the shell S_1 reverses its direction. This is consistent with our conclusions based on $C^{12}(t)$. We note that $C_{12}(t)$ remains negative certainly until $t \sim 0.9$. As suggested above, we infer that this negative momentum of the shell prolongs the 'negative' regime of the macf, (i.e., $C_p(t) \equiv C_{11}(t)$). The insert in Figure 2(a) compares the x-component of $C_{12}(t)$ for two system sizes, $N = 256$ and $N = 500$, revealing a statistically small N-dependence in this function.

We present $C_{23}(t)$ in Figure 2(b), which is the momentum transfer cross correlation function between shells, S_1, and S_2, for the state point $\rho = 0.8$ and $T = 1.9$. This

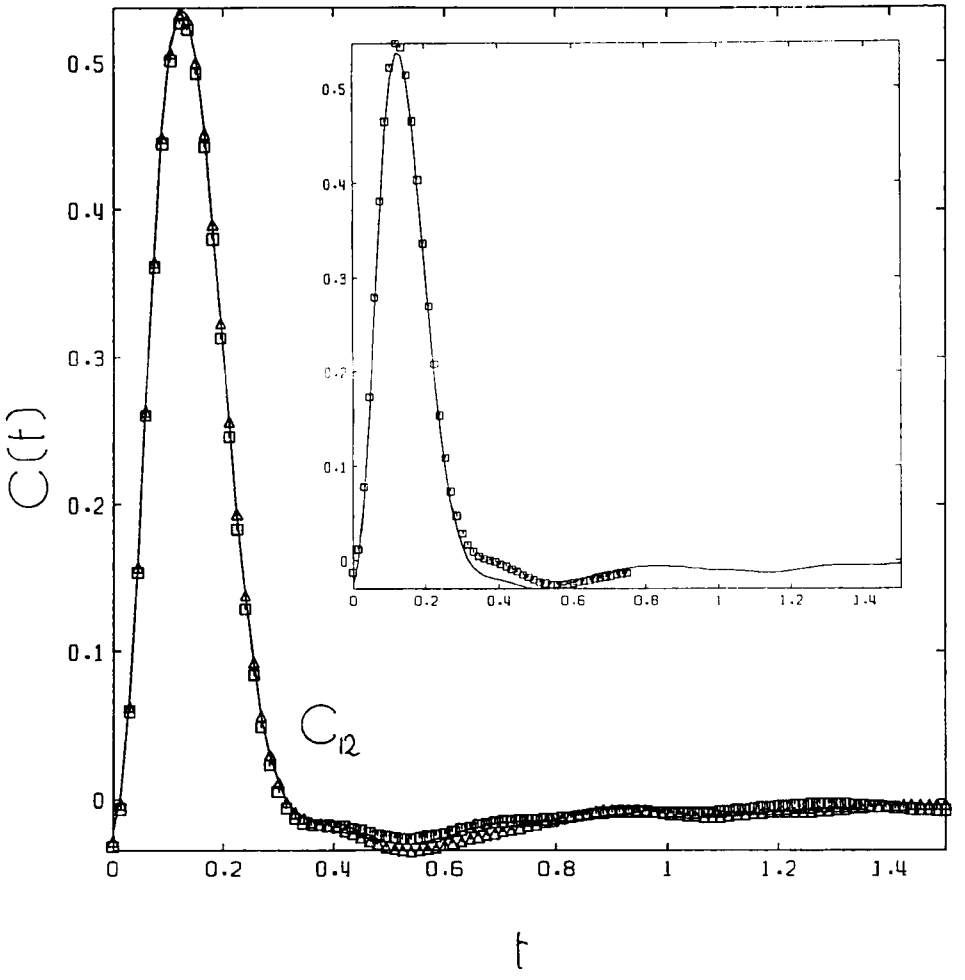

Figure 2(a) The time cross-correlation functions $C_{12}(t)$, for the x, solid line, y, □, and z, △ components at the 3D *LJ* $N = 256$ state $\rho = 0.8442$, $T = 0.722$, $\dot{\gamma} = 0$, $r_a = 0.85$, $r_b = 1.3$ and $r_c = 1.6$. The insert shows the x component of $C_{12}(t)$, for $N = 256$, solid line, and $N = 500$, □.

function reveals aspects of the transfer of momentum through the first coordination shell around a test particle (i.e., from S_1 to S_2). In the insert to Figure 2(b) we also show $C_p(t)$ and $C_{12}(t)$ for the same state point. We note that at this lower density state point, there is no negative lobe in the MTCCF at $T \simeq 0.3$. Instead $C_{12}(t)$ and particularly, $C_{23}(t)$, have a long time positive tail, reflecting less efficient back-scattering of the component particles between each cage. A comparison with $C_{12}(t)$ from the $\rho = 0.8442$ and $T = 0.722$ (Figure 2(a)) state point demonstrates the shells transmit (rather than reflect) more of the momentum at $\rho = 0.8$ and $T = 1.9$ (Figure

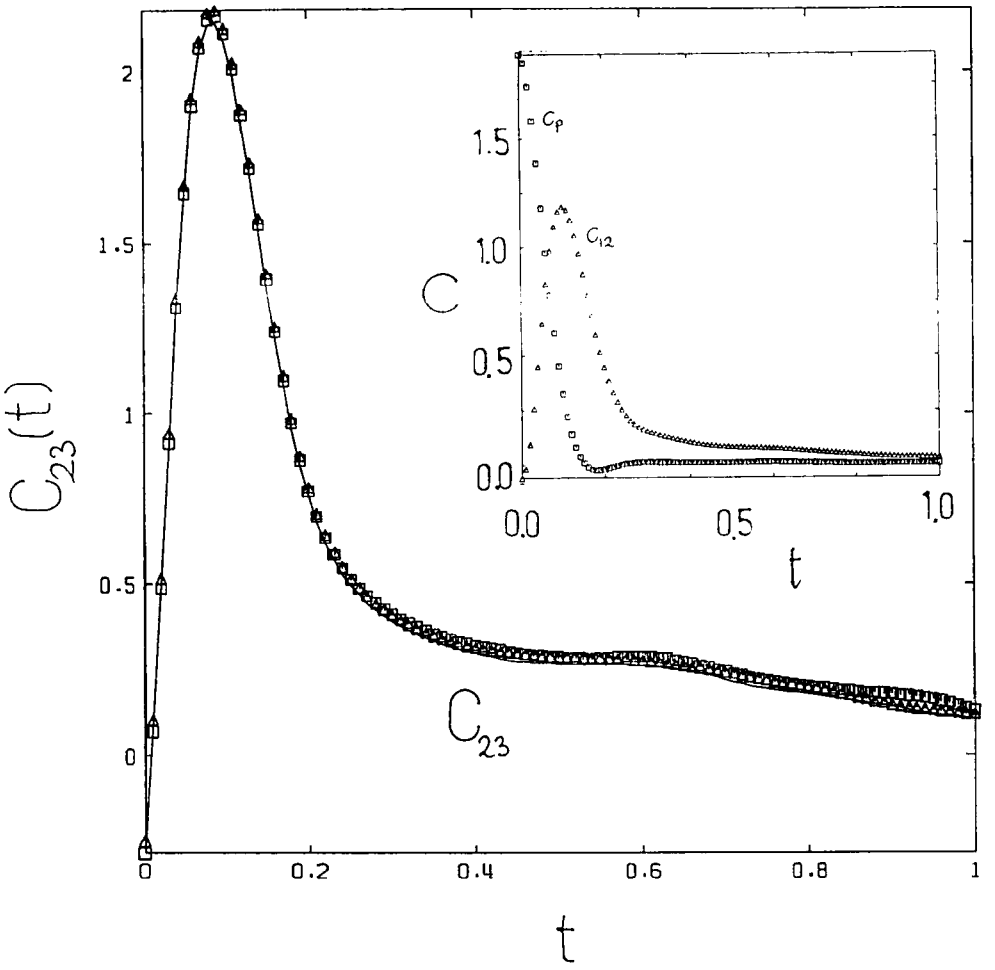

Figure 2(b) The $C_{23}(t)$ for the x, solid line, y, □, and z, △ components at $\rho = 0.8$ and $T = 1.9$. The insert shows the x-component of $C_p(t)$ and $C_{12}(t)$.

2(b)). Figure 2(c) compares $C_{13}(t)$ and $C_{23}(t)$ for $\rho = 0.8442$ and $T = 0.722$. $C_{23}(t)$ in comparison with $C_{12}(t)$ does not have a negative lobe at $t \simeq 0.3$. The momentum from shell 2 is less efficiently backscattered from shell 1 than is the momentum of the central particle from shell 1. C_{13} manifests a peak at $t \simeq 0.3$ reflecting the passage of momentum from the central particle through shell 1 to shell 2.

As we consider the functions $C^{12}(t)$ and $C_{12}(t)$, we lose progressively more direct information about the dynamics of the central particle. They inform us more about the effect of the central particle on the 'state' of the surrounding shells of atoms. This trend is continued in the function, $C_{22}(t)$, the shell-shell correlation function calculated for the first time here. An example of $C_{22}(t)$ is shown in Figure 3, for the near triple point state point. S_1's initial momentum decreases largely as the macf until $t \sim 0.2$, when a 'shoulder' appears on $C_{22}(t)$, indicating a slowing down of the momentum

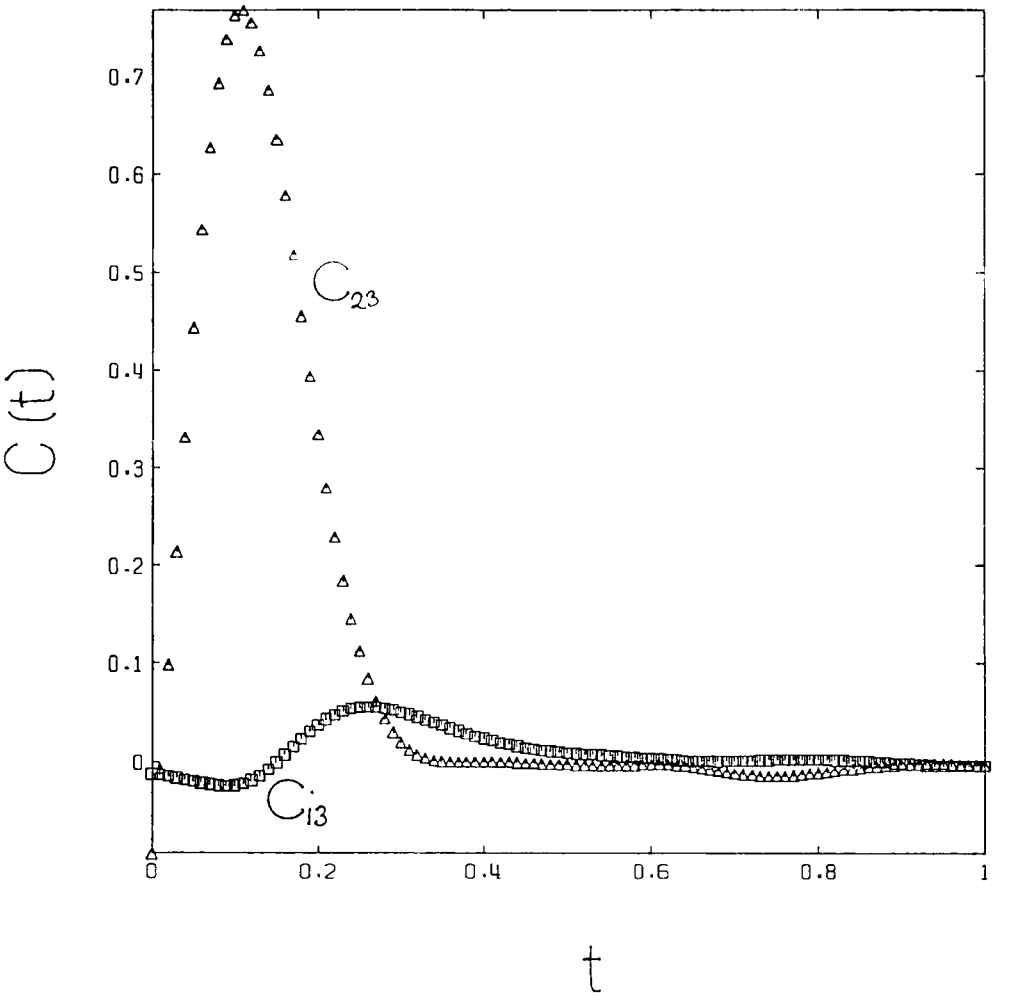

Figure 2(c) A comparison between $C_{13}(t)$ (□) and $C_{23}(t)$ (△) for $\rho = 0.8442$, $T = 0.722$, $\dot{\gamma} = 0$.

relaxation of the shell. Of all particles, the central particle will have the most influence on the shell, S_1, because it is on average nearest to each shell 1 particle. The motion of the central particle within its cage imposes an additional correlation time on the fluctuations of the shell, at times corresponding to the 'collision' time of the particle with S_1, which we can extract from the macf. (The direct transfer of momentum to the cage we consider to be insignificant in this process.) As the central particle oscillates between the centre to the boundary of its shell, the shell experiences a variation in potential energy, suffering periodic accelerations and retardations of its dynamical evolution. Note that we cannot be certain where the central particle is at the point of the shoulder in $C_{22}(t)$, but suggest that it is in the middle of the shell—so that it will slow down the dynamics of the whole shell uniformly at this position.

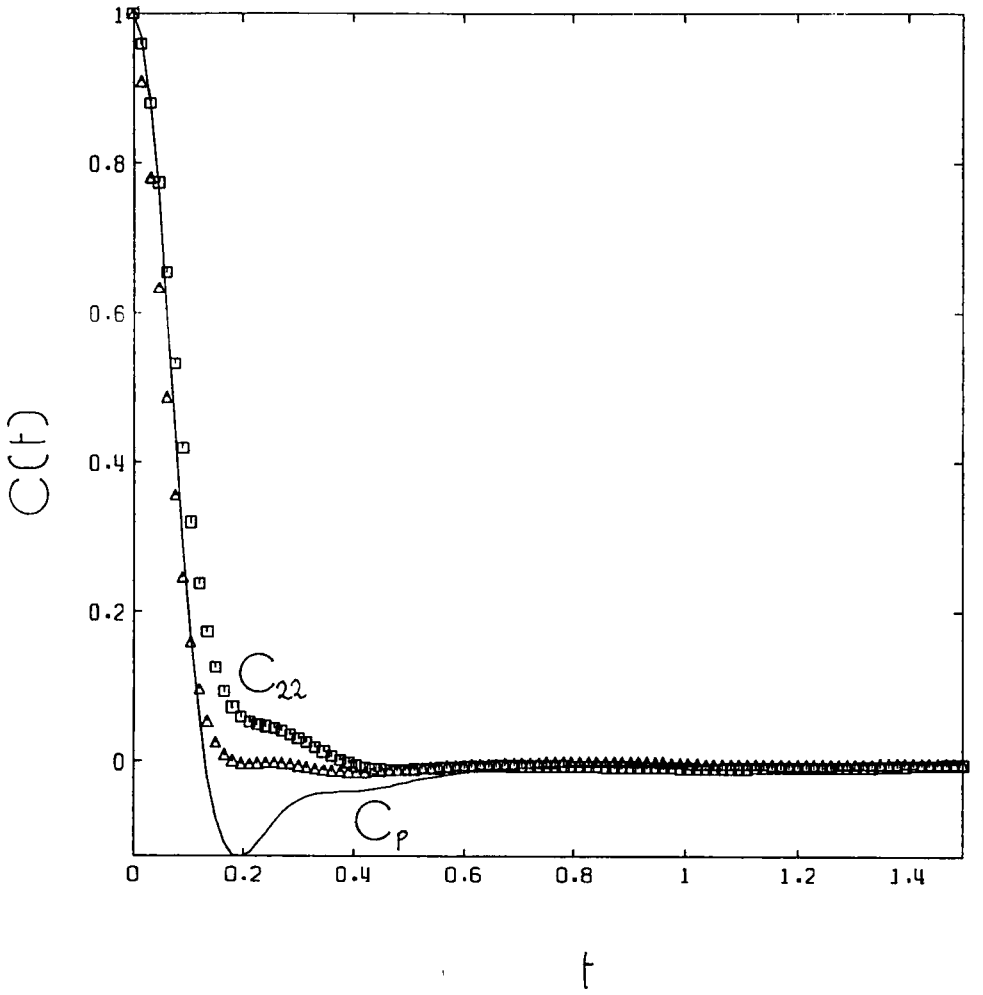

Figure 3 The time cross-correlation functions, x components, $C_p(t)$, solid line, $C_{22}(t)$, □ and $C_{33}(t)$, △. at the 3D *LJ* $N = 256$ state $\rho = 0.8442$, $T = 0.722$, $\dot{\gamma} = 0$, $r_a = 0.85$, $r_b = 1.3$ and $r_c = 1.6$.

The second shell momentum autocorrelation function, $C_{33}(t)$ (shown also in Figure 3) decays even more rapidly at short time than, $C_{22}(t)$ because its more abundant neighbours hasten the momentum transfer process. Only slight evidence of a shoulder appears near $t = 0.3$. This suggests that the modulation of the dynamics of the second shell, S_2 atoms, portrayed in $C_{33}(t)$, is considerably reduced over that in the first shell, S_1. This is reasonable, as the second shell is further away from the central particle than the first shell and its dynamics are therefore influenced primarily by its nearest neighbours, namely the first and third shell atoms around the central particle. This is consistent with the $C_{23}(t)$ results shown in Figure 2.

We now consider the normalised **relative** momentum correlation functions, $C^{12}(t)$, $C^{13}(t)$ and $C^{23}(t)$ in Figure 4. Here we investigate the motion of the central particle

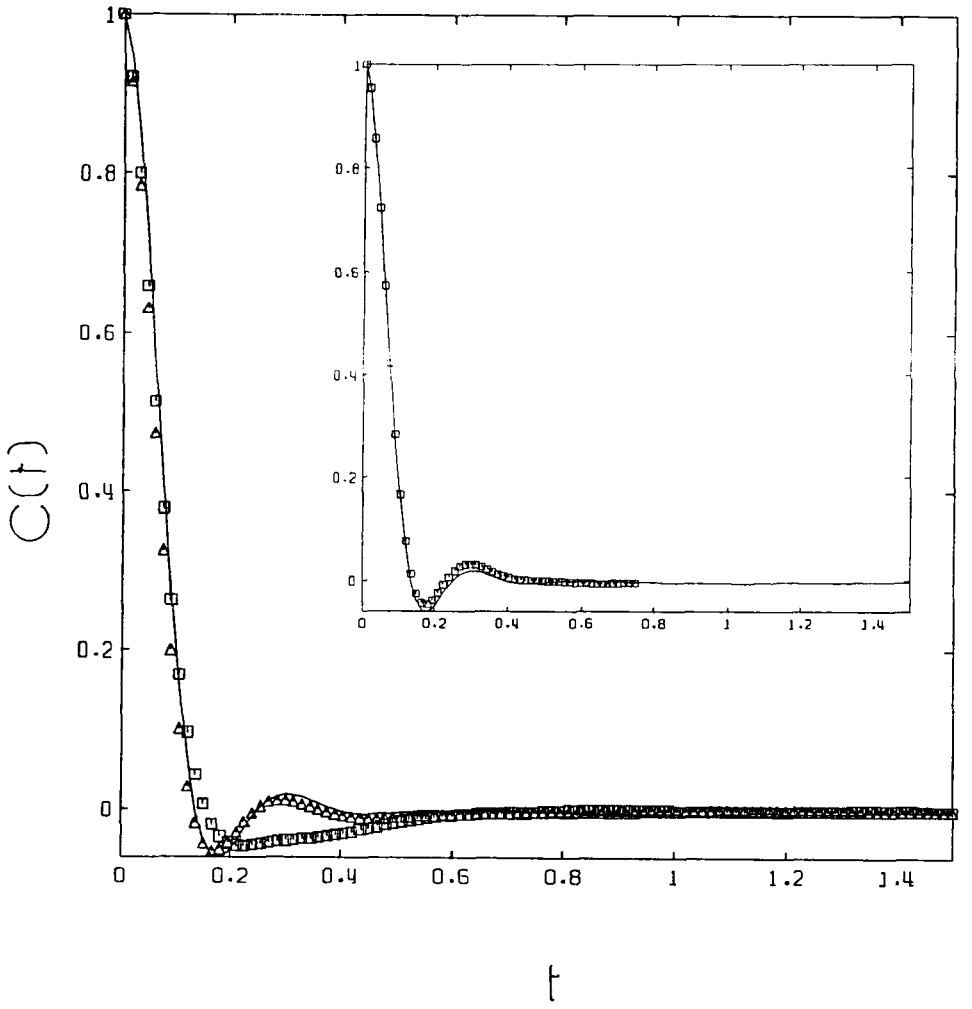

Figure 4 The time cross-correlation functions, x components, $C^{12}(t)$, solid line, $C^{13}(t)$, □ and $C^{23}(t)$, △ for the same state point as for Figure 1–3. The insert shows the x component of $C^{12}(t)$, for $N = 256$, solid line, and $N = 500$, □.

with respect to its shells, S_1 and S_2, and with the two shells with respect to one another, respectively. These three functions are statistically indistinguishable at times, $t < 0.13$. The $C^{12}(t)$ and $C^{23}(t)$ agree essentially over the entire time span. This is macf, which indicates the modulation of the shell dynamics by the quasi-oscillations the '13' particle combinations are much further apart, as noted above. We have already discussed $C^{12}(t)$ and it only remains for us to interpret the distinct features of $C^{13}(t)$. All of these functions go negative at a time ~ 0.15, reflecting (at least initially) principally a reversal in the momentum of the central particle. This behaviour is manifest in the $C^{13}(t)$ at a later time. There is no return to positive values for $C^{13}(t)$, as it has a long time negative tail. This suggest that there is no reversal of the

momentum of shell 2 since its reversal would lead to a positive region in $C^{13}(t)$. The long time tail in $C^{13}(t)$ is, not surprisingly, taking on the form of the macf at long times therefore. In fact, for $r_c \to \infty$ we have $C^{13}(t) \to C_p(t)$. This is because the further removed the shell is from the central particle, the less correlation there is between them. The relative momentum then simply becomes the momentum of the central particle.) In order to show that the structure in $C^{12}(t)$ is not a simulation artefact, computations were carried out for $N = 500$ as well as $N = 256$. The $C^{12}(t)$ from these simulations are presented in the insert of Figure 4. The second positive peak in this function is still pronounced for $N = 500$, thus vindicating the method and parameters.

We now report our investigations of the relaxation of the stress about the central particle. (Momentum correlation functions give limited information as the 'angular' and 'longitudinal' fluctuations of the cage are not resolved.) In Figure 5 we show

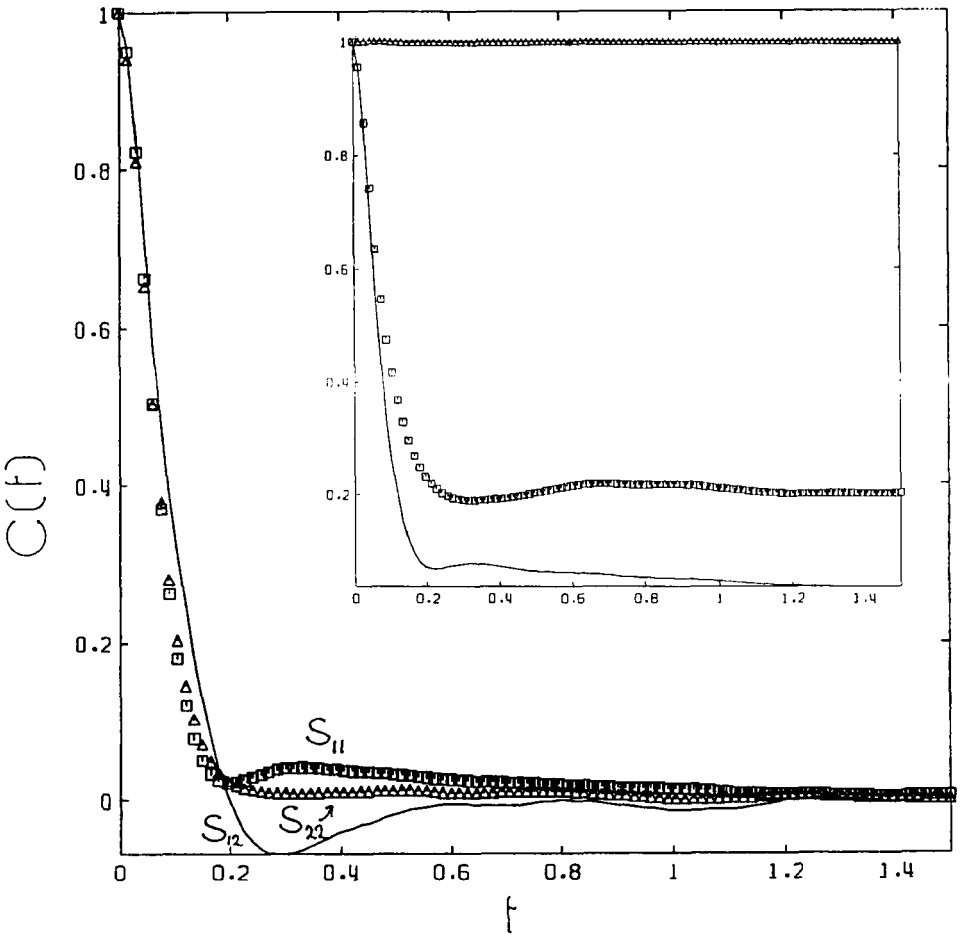

Figure 5 The time cross-correlation functions, XY components of, $S_{12}(t)$, solid line, $S_{11}(t)$, □ and $S_{22}(t)$, Δ for the same state point as for Figure 1–3. The insert shows the corresponding XX components.

the XY component of the normalised $S_{11}(t)$, $S_{12}(t)$ and $S_{22}(t)$ for the near triple point state point. The single particle stress-stress autocorrelation function, $S_{11}(t)$, shows evidence of the cage-rebound, which is absent in $S_{22}(t)$. The $S_{11}(t)$ follows the macf in form (but does not go negative), indicating that at short time the stress relaxation is 'radial' rather than 'reorientational', as has been ascribed to long time shear stress relaxation[11]. Only the magnitude of the stress changes, through the $d\phi(r)/dr$ term in Eq. (15). The reorientational term is probed through the $x_{1j}y_{1j}$ component of Eq. (15), which we propose does not change significantly on this time scale. The surrounding atoms do not significantly change in relative orientation during the time scale of the macf. $S_{12}(t)$, on the other hand, has a deep negative minimum at $t = 0.29$. This indicates that the central particle's shear stress, and the cage, S_1's stress, change sign as the central particle 'oscillates' in its (moving) cage. Figure 5 also shows

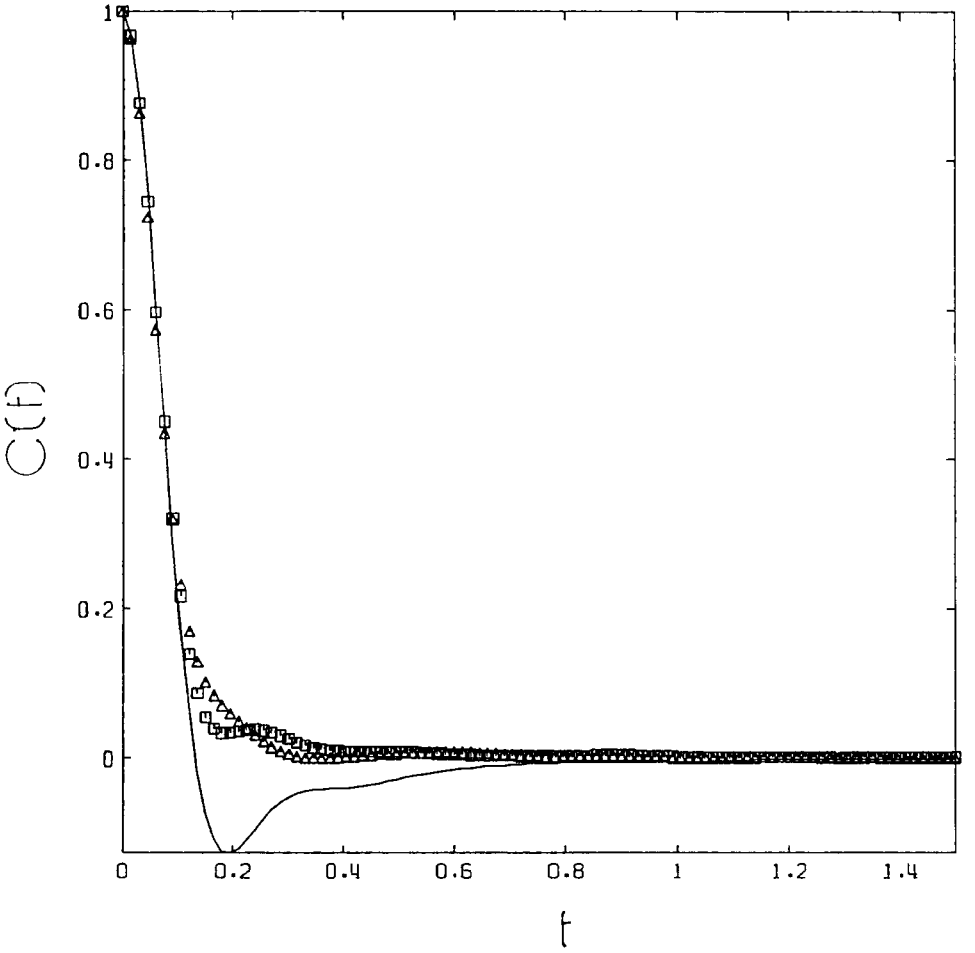

Figure 6 The time cross-correlation functions, X components of, $C_p(t)$, for $\dot{\gamma} = 0$, solid line, for $\dot{\gamma} = 1$, □ and for $\dot{\gamma} = 2$, △ for the same state point as for Figure 1–3 with $N = 256$.

that $S_{22}(t)$ is similar to $S_{11}(t)$ at short time but lacks the peak at $t \simeq 0.3$, demonstrating (yet again) the reduced influence of the central particle on shell 2 when compared to its influence on shell 1.

The superposition of a shear flow can have a dramatic effect on the single-particle dynamics if the response is noticeably non-Newtonian. We consider a range of shear rates, $\dot{\gamma}$ which cause the fluid to depart from being a Newtonian liquid ($\dot{\gamma} \to 0$) to being approximately up to 50% shear thinned, i.e., for $\dot{\gamma} = 0$, 1, 2 we have $\eta = 3.5$, 2.1, 1.6[19]. An example of the effect of the shear on the peculiar macf for $\dot{\gamma} = 0$, 1 and 2 is shown in Figure 6. It indicates that the shear flow progressively reduces the backscattering of the central particle (which is hardly evident at $\dot{\gamma} = 2$). This appears in the progressive diminution of the negative lobe in the macf as shear rate increases.

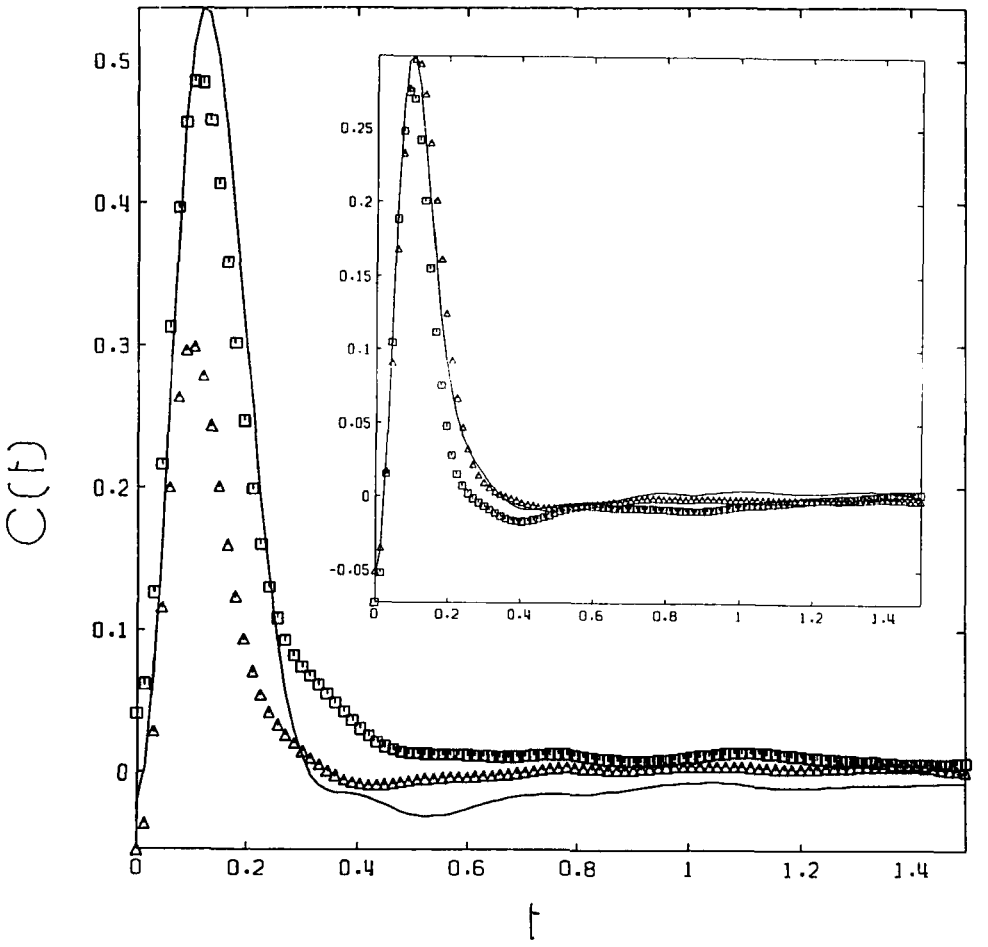

Figure 7 The time cross-correlation functions, x components of $C_{12}(t)$, for $\dot{\gamma} = 0$, solid line, for $\dot{\gamma} = 1$, □ and for $\dot{\gamma} = 2$, △ for the same state point as for Figure 1–3. The insert shows the components, x, solid line, y, □ and z, △ for the $C_{12}(t)$, $\dot{\gamma} = 2$ and $N = 256$.

In Figure 7 we show the x component of the momentum transfer cross-correlation function, $C_{12}(t)$, for $\dot{\gamma} = 0$, 1 and 2. It indicates that as the shear rate increases less momentum is transferred to the first shell at short time (i.e., $t < 0.2$) and that there is a slowly damped decay of momentum transfer at longer times (which is not there at $\dot{\gamma} = 0$). This is consistent with a distorted first shell, S_1, of ellipsoidal shape with its principal axis at approximately 45° to the x and y axes. The first coordination shell loses its spherical symmetry and provides a less well-defined cage for central particle collisions. The central particle has further to travel along the principal axis of the ellipsoid, but less time along the short axis of the ellipsoid. There is therefore in a shear field a greater spread of collision times. The times to the peaks of the momentum transfer function $C_{12}(t)$ for $\dot{\gamma} \neq 0$ are slightly *less* than that for the $\dot{\gamma} = 0$ case. The momentum transfer appears in the $\dot{\gamma} \neq 0$ case to be occurring first

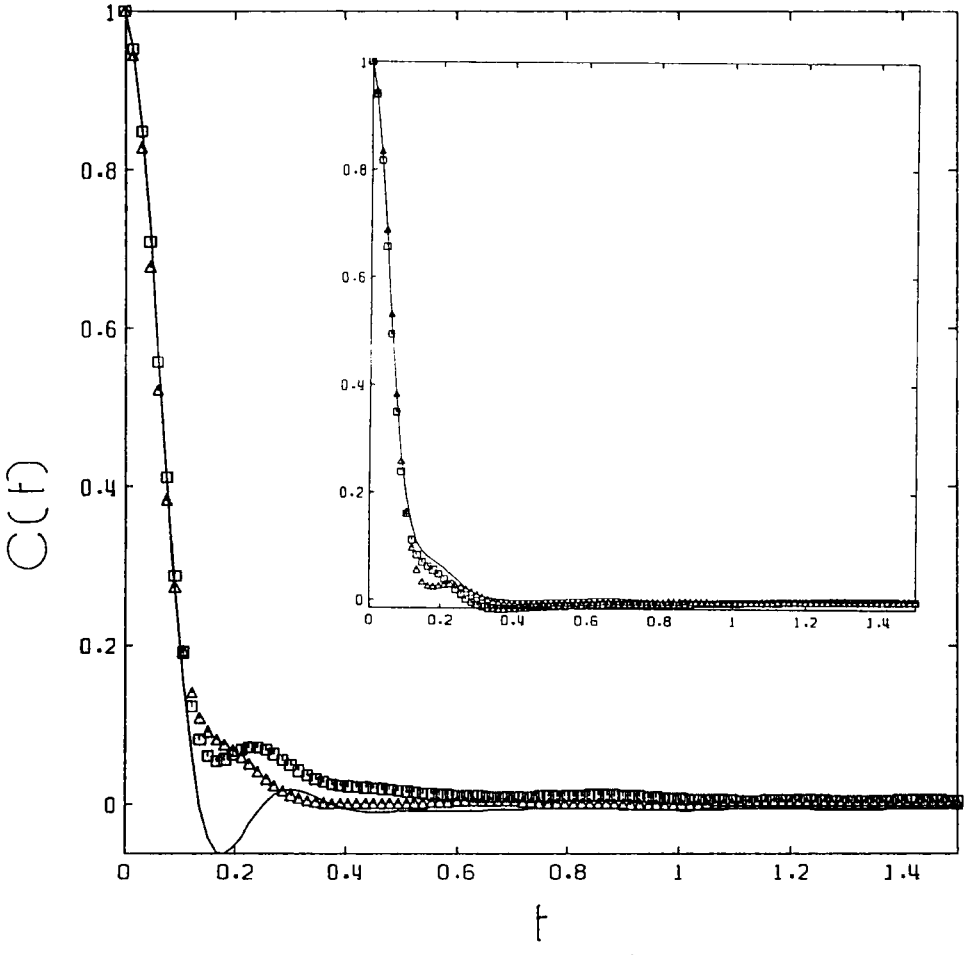

Figure 8 The time cross-correlation functions, x components of $C^{12}(t)$, for $\dot{\gamma} = 0$, solid line, for $\dot{\gamma} = 1$, □ and for $\dot{\gamma} = 2$, △ for the same state point as for Figure 1–3. The insert shows the components, x, solid line, y, □ and z, △ for the $C_{12}(t)$, $\dot{\gamma} = 2$ and $N = 256$.

primarily along the minor axis of the distorted ellipsoidal S_1. The central particle, while moving down the length (minor-axis) of the ellipsoidal shell, will encounter its 'sides' sooner than from the original spherical shell. This time will decrease with increasing $\dot{\gamma}$, as the ratio of the major-to-minor axes increases, i.e., the sides get closer to the central particle. The decrease in magnitude of the transferred momentum suggests the motion is, on the average, more probable along the major-axis. There is evident a long-time tail in the x component of $C_{12}(t)$, which increases with shear rate, which we attach to collisions with S_1 along the major axis. Note that the heights of the peaks of $C_{12}(t)$ decrease with increasing $\dot{\gamma}$, reflecting this spread of collision times.

The insert of Figure 7 shows the x, y and z components of $C_{12}(t)$ at $\dot{\gamma} = 2$. The diminution in the intensity of momentum transport between the impurity and S_1 is similar in all directions because the first shell particles are 'stretched' around a surface

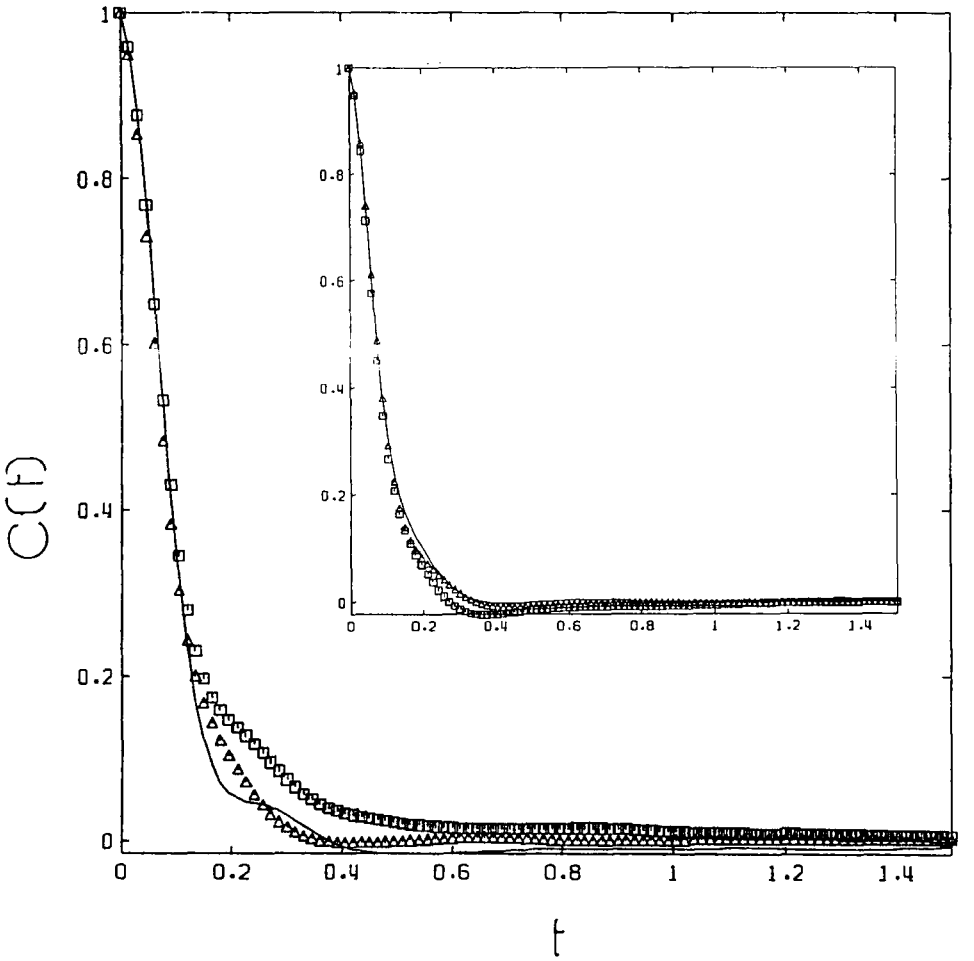

Figure 9 As for Figure 8, except the time correlation functions, x components of $C^{22}(t)$, are given.

of greater surface area when the first shell is distorted from a spherical shell to an ellipsoid. Even along the contracted minor-axis, 'hard' collisions occur less frequently than collisions in the spherical S_1.

In Figure 8 we show the x-component of $C^{12}(t)$ for $\dot{\gamma} = 0$, 1 and 2, which has the overall appearance of $C_p(t)$ for the same states. The insert gives the three cartesian components of $C^{12}(t)$ for $\dot{\gamma} = 2$. This figure shows clearly that there is severe reduction in the number of velocity reversing collisions in a shear thinned fluid. This is perhaps the microscopic origin of the increase in diffusion coefficient with increasing shear rate. Also the insert of Figure 8 shows that the three cartesian components of $C^{12}(t)$ are statistically different. This is because the shear flow field causes structural distortion to occur in the fluid that is different in the three cartesian directions.

In Figure 9 we show $C^{22}(t)$ for $\dot{\gamma} = 0$, 1 and 2. There is a comparitively long-time tail for $\dot{\gamma} = 1$ but not for higher shear rates, illustrating the complex dynamical relaxation induced as shear rate increases. The distinct shoulder at $t \sim 0.2$–0.3 evident at $\dot{\gamma} = 0$ disappears at the finite shear rates considered here. The insert gives the three cartesian components of $C^{22}(t)$ for $\dot{\gamma} = 2$. Figure 9 illustrates that the central particle has a strong influence on the dynamics of its cage (S_1, here) for longer times as shear rate increases, resulting from the wider spread of collision times between the central particle and its surrounding cage of atoms (i.e., in S_1).

4 CONCLUSIONS

In this work we have brought out some new features of the interaction between a particle and its surrounding first shell of neighbours in the liquid state. We show that beyond the first minimum of the vacf, the first shell is moving faster than the central particle in the same ('reverse') direction. We show that the first shell momentum autocorrelation function has a shoulder beyond the first minimum in the macf, which indicates the modulation of the shell dynamics by the quasi-oscillations of the central particle contained within it. The short time dynamics ($t < 0.2$) is governed by correlated backscattering collisions with a persistence of the initial vector betweeen the pair colliding. At longer times there is a transition to a hydrodynamic regime in which the vector changes more rapidly than the scalar distance between the pair.

The effect of shear is to spread out the range of collision times between the central particle and the first shell. The effectiveness of the momentum transfer to the particle's first shell is also reduced. This is manifest in a disappearance of the minimum in the macf and a smaller peak and 'spreading out' of the momentum transfer cross-correlation function.

Acknowledgements

D.M.H. gratefully thanks *The Royal Society* for the award of *a Royal Society 1983 University Research Fellowship*. W.G.S. thanks The Naval Research Laboratory, Washington, DC, USA, for sponsoring the collaboration. We thank S.E.R.C. for the award of computer time at the University of London Computer Centre, and the RHBNC Computer Center for use of their VAX 11/780 computer facilities.

References

1. A. Rahman, *Phys. Rev.*, **136A**, 405 (1964); *J. Chem. Phys.*, **45**, 2585 (1966).
2. S. Franchetti, *Il. Nuovo Cim.*, **42B**, 85 (1977).
3. B. J. Alder and T. E. Wainwright, *Phys. Rev. A*, **1**, 18 (1970).
4. T. Gaskell and S. Miller, *J. Phys. C*, **11**, 3749 (1978); *ibid*, **11**, 4839 (1978).
5. See P. E. Mason and T. Gaskell, *Mol. Phys.*, **41**, 529 (1980); T. Gaskell and P. E. Mason, *Phys. Lett.*, **11A**, 34 (1980), and T. Gaskell, *J. Phys. Cond. Matt.*, **1**, 6203 (1989) and references quoted therin.
6. Y. Endo and H. Endo, *J. Chem. Phys.*, **80**, 2087 (1984).
7. P. T. Herman and B. J. Alder, *J. Chem. Phys.*, **56**, 987 (1972).
8. S. W. Haan, *Phys. Rev. A*, **20**, 2516 (1979).
9. H. A. Posch, U. Balucani and R. Vallauri, *Physica*, **123A**, 516 (1984).
10. T. Ichimura, N. Ogita and A. Ueda, *J. Phys. Soc. Japan*, **45**, 252 (1978).
11. A. J. C. Ladd, W. E. Alley and B. J. Alder, *J. Stat. Phys.*, **48**, 1147 (1987).
12. D. P. Dean and J. N. Kushick, *J. Chem. Phys.*, **78**, 619 (1982).
13. U. Balucani, R. Vallauri and C. S. Murthy, **77**, 3233 (1982).
14. T. Tsang and H. Tang, *Phys. Rev. A*, **15**, 1696 (1977).
15. C. S. Murthy and K. Singer, *J. Phys. Chem.*, **91** 22 (1987).
16. R. J. Speedy, F. X. Prielmeier, T. Vardag, E. W. Lang and H. D. Ludemann, *Mol. Phys.*, **66**, 577 (1989).
17. U. Balucani, R. Vallauri, T. Gaskell and M. Gori, *Phys. Lett.*, **102A**, 109 (1984).
18. T. Gaskell and P. E. Mason, *J. Phys. C*, **14**, 561 (1981).
19. D. M. Heyes, *J. Chem. Soc., Farad. Trans. 2*, **82**, 1365 (1986).
20. D. J. Evans and G. P. Morris, *Phys. Rev. A*, **30**, 1528 (1984).
21. K. D. Hammonds and D. M. Heyes, *J. Chem. Soc. Farad. Trans. 2*, **84**, 705 (1988).
22. C. S. Murthy and K. Singer, *Proc. Roy. Soc.*, **389A**, 299 (1983).
23. U. Balucani and R. Vallauri, *Chem. Phys. Lett.*, **74**, 75 (1980).
24. U. Balucani, R. Vallauri and C. Murthy, *Phys. Lett.*, **84A**, 133 (1981).
25. U. Balucani, R. Vallauri, C. Murthy, T. Gaskell and M. S. Woolfson, *J. Phys. C*, **16**, 5605 (1983).
26. U. Balucani, R. Vallauri, T. Gaskell and M. Gori, *J. Phys. C*, **18**, 3133 (1985).
27. U. Balucani, M. Gori, R. Vallauri, *Chem. Phys. Lett.*, **119**, 152 (1985).
28. M. P. Allen and D. J. Tildesley, *Computer Simulation of Liquids*, (Oxford Science Publications, 1989).
29. W. C. Sandberg, T. A. Litovitz and C. J. Montrose (to be submitted.)